Analysis of the relationship between yield in cereals and remotely sensed fAPAR in the framework of monitoring drought impacts in Europe

Carmelo Cammalleri, Niall McCormick, Andrea Toreti

European Commission, Joint Research Centre (JRC), 21027 Ispra (VA), Italy.

Correspondence to: Carmelo Cammalleri (carmelo.cammalleri@ec.europa.eu)

Abstract. This study focuses on the relationship between satellite-measured fAPAR (Fraction of Absorbed Photosynthetically Active Radiation) and crop yield cereals in Europe. Different features of the relationship between annual yield and multiple time series of fAPAR, collected during different periods of the year, were investigated. The two key outcomes of the analysis are the identification of the period: i) from March to October as the one having the highest positive correlation between fAPAR and yield; ii) from February to May as the period characterized by most of the estimated negative correlation. While both periods align well with the commonly assumed dynamic of the growing season, spatial differences are also observed across Europe. On the one hand, the Mediterranean regions report the highest correlation values ($r > 0.8$) and the longest continuous periods with positive statistically significant results (up to 7 months), covering most of the growing season. On the other hand, the central European region is characterized by the most limited positive correlation values, with only 2 months or less showing statistically significant results. While marked differences on the overall capability to capture the full dynamic of yield are observed across Europe, fAPAR anomalies seem capable to discriminate low yield years from the rest in most of the cases.

Keywords: vegetation indices, agricultural drought, EDO, CEMS.

1. Introduction

Drought is a multifaceted phenomenon threatening societies, economies and ecosystems in a complex web of cascading effects (UNDRR, 2021). Amongst the major sectors that are impacted by drought, agriculture is still recognized as the most sensitive one (FAO, 2015; FAO et al., 2018; FAO, 2021), as reflected by the large share of reported impacts for agriculture over the majority of countries and drought events in Europe (Stahl et al., 2016).

Most drought monitoring systems recognize the prominent role of agricultural drought, by refining indicators of meteorological drought in order to better account for impacts on vegetation growth (e.g. the Standardized Precipitation-Evapotranspiration Index – or SPEI; Vicente-Serrano et al., 2012), and/or by directly incorporating drought indicators that are based on remotely sensed vegetation indices (WMO and GWP, 2016). In particular, negative deviations from climatological values of satellite measurements of vegetation "greenness" – for example, the standardized anomalies of the fraction of Absorbed Photosynthetically Active Radiation (fAPAR) that are provided by the European and Global Drought Observatories (EDO and GDO, https://edo.jrc.ec.europa.eu) – are often adopted as a proxy variable for the adverse effects of drought on vegetation.

While such approaches are logically based on the connection between reduced vegetation greenness and diminished plant productivity, it is also well known that droughts occurring during different phenological stages may have different impacts on yield and production (i.e. Barros et al., 2021; Ceglar et al., 2020; Chaves et al., 2002; Demirevska et al., 2009; Monteleone et al., 2022; Stallmann et al., 2020; Zampieri et al., 2017). Consequently, greenness anomalies are not always directly related to reduction in yield, depending on the development stages of the vegetative cycle when they manifest. Some studies have tried to account for this concept by limiting the analysis to the growing period and excluding data for the plant dormancy phase (e.g. Rojas et al., 2011), by deriving key variation metrics (i.e. amplitude, integral, maximum) from the full growing season (e.g. Kang et al., 2018), or by focusing only on key periods (i.e. a specific month) that have been shown to correlate well with deviations in annual yield for a given study area (Bachmair et al., 2018).

Within the framework of the near real-time monitoring of drought events, the task of evaluating and quantifying the actual relevance of an observed anomaly in vegetation greenness is complicated by the need to update continuously the status based on newly acquired data, without the benefit of the full picture of the complete vegetation cycle. This limits the possibility to implement some of the above-mentioned approaches as part of

59 operational drought monitoring systems, other than the simple masking of data acquired
60 outside of a pre-defined period (e.g. the growing season). An example of an early warning
61 system that accounts for the timing of the observed anomalies is the Anomaly Hot Spots of
62 Agricultural Production (ASAP) decision support system (Rembold et al., 2019), where the
63 seasonal progression (expansion, maturity, senescence) is explicitly considered in determining
64 the warning level.

65   As part of the shift in the drought risk management paradigm from a reactive to a
66 proactive approach, the move from simple hazard indicators to quantitative assessments of
67 risk and impacts is likely to be further integrated within modern early warning systems
68 (UNDRR, 2021). In this regard, independent estimates of actual drought impacts, such as the
69 information that can be derived from records of yield deviations for different crop types,
70 constitute a valuable reference. Unfortunately, these information are often collected at coarse
71 spatial resolution and they are available with a significant temporal delay. They are however
72 very valuable to assess if anomalies in vegetation indices can be used to detect the effects of
73 drought conditions, and how their robustness as proxy of yield reduction varies in space and
74 throughout the year. This can also enable the successive evaluation of the efficiency of
75 remotely sensed indicators as a proxy for the effect of drought on vegetated land, and the
76 refinement of their use as stress-forcing data for agro-economic models, for the assessment of
77 losses in agriculture due to droughts (García-León et al., 2021).

78   In this context, the primary goal of this study is to analyse to what extent the year-by-
79 year dynamics of yield in Europe can be explained by a regularly updated operational
80 vegetation drought indicator, in particular by the fAPAR anomalies produced by EDO. Yield
81 data for cereals, recorded by Eurostat, are here used as a starting quantity to produce records
82 of anomalies in yield at European scale. The spatio-temporal variations in the relationship
83 between dekadal (i.e. 10-day) fAPAR anomalies and yearly yield deviations can help in
84 identifying the periods of the year when fAPAR represents a reliable proxy information of
85 yield reduction impacts in Europe. This would prove a quantitative basis for improving the
86 assessment of drought impacts in agriculture, with potential benefits both for drought
87 monitoring systems and for agro-economic models.

88 **2. Material and Methods**

89 **2.1 Eurostat yield dataset**

90 Eurostat, the European Statistical Office, publishes regular reports of statistics on annual
91 crops, including data on production, cultivated area and yield for different crop types, at both

92 national and sub-national aggregation levels (Eurostat, 2020), with the aim of providing a
93 harmonized database of data collected by EU Member States and neighbouring countries.

94 For the purposes of this study, annual yield data of cereals (wheat and spelt, rye, barley,
95 oats, grain maize, triticale, and sorghum) have been retrieved between 2001 (first full year
96 with available fAPAR data) and 2018 (last available year in the Eurostat database at the time
97 of this study), mostly at the spatial scale of Eurostat's so-called "NUTS 2" regions (hereafter
98 referred to simply as regions). Only in the case of Germany and the UK, data at the NUTS 1
99 level were used, in order to maximize both data coverage and consistency in region size with
100 the rest of the domain.

101 Since yield data are to be used for computation of deviations from the long-term
102 average, temporal consistency in the data records is essential. For this reason, records that are
103 flagged by Eurostat as estimated, provisional, unreliable or with a definition that differs due to
104 missing components, were excluded from the analysis.

105 Systematic changes in the annual yield time series were removed by applying a
106 Savitzky–Golay filter to account for advancement in technology and crop management
107 (Tadesse et al., 2015), before standardized anomalies were computed only for those regions
108 with more than 9 years of data (i.e. half of the analyzed period). A linear de-trending was also
109 tested (not shown), but a limited effect of this choice was observed on the obtained yield
110 anomalies time series. Following this procedure, 240 regions with valid time series were
111 obtained (out of the 267 regions considered at the start of the study).

112 **2.2 MODIS fAPAR dataset**

113 The fraction of Absorbed Photosynthetically Active Radiation (fAPAR) is one of the 50
114 Essential Climate Variables recognized by the UN Global Climate Observing System
115 (GCOS), mainly thanks to its direct relationship with primary production
116 (https://gcos.wmo.int/en/essential-climate-variables/fapar).

117 fAPAR, and in particular its deviations from historical climatology, constitutes the ideal
118 proxy variable for the effects of drought on vegetated lands (Rossi et al., 2008). In this
119 context, remote sensing images collected by the MODIS (MODerate resolution Imaging
120 Spectroradiometer) sensor represent a unique data source for drought studies, due to the
121 unprecedented longevity of the Terra satellite.

122 In this study, the standard MODIS Terra LAI/fAPAR product (i.e. MOD15A2H,
123 Collection 6) is used (Myneni, 2015), in which global fAPAR maps are derived from the
124 atmospherically corrected Bidirectional Reflectance Distribution Function (BRDF) recorded

125 by MODIS in 7 spectral bands, by solving the three-dimensional radiation transfer process
126 through a look-up-table approach (Knyazikhin et al., 1998; Wang et al., 2001).

127 The standard MODIS product is distributed as 8-day composites (using a maximum
128 composite method) at a spatial resolution of 500-m in 1,200 × 1,200 km tiles on a sinusoidal
129 grid. Data include a quality assessment (QA) layer that allows to detect where the simplified
130 back-up algorithm has been used.

131 Datasets of both fAPAR and fAPAR anomalies based on MOD15A2H raw data are
132 regularly produced as part of the European and Global Drought Observatories (EDO and
133 GDO, https://edo.jrc.ec.europa.eu) of the EU's Copernicus Emergency Management Service.
134 The operational fAPAR dataset is obtained after a set of pre-processing procedures, including:
135 1) screening of the low-quality data based on the QA flag layer; 2) spatial aggregation of the
136 data (simple average) at 1-km resolution and re-projection onto a lat/lon regular grid at 0.01°
137 resolution with nearest neighbour resampling; 3) temporal aggregation at dekadal scale (three
138 maps per month: days 1–10, 11–20 and 21–end-of-month) by means of a weighted average of
139 the two closest 8-day images (weight proportional to the overlapping with the dekadal
140 period); and 4) exponential temporal smoothing of the dekadal data (with smoothing
141 parameter equal to 0.5; Brown and Meyer, 1961).

142 Here, the fAPAR anomalies were computed as standardized deviations from the
143 reference period (2001-2018), only if at least 6 years of data were available and only where
144 the long-term standard deviation was greater than 0.01 (to exclude areas of low variability,
145 such as deserts or highly stable densely vegetated areas). The reference period of 2001-2018
146 is consistent with the one used for yield anomalies.

147 **2.3 Analysis strategy**

148 In this study, the analysis of the relationship between the dekad time series of fAPAR
149 anomalies and yearly crop yield is based primarily on the Spearman correlation coefficient
150 (r). In order to carry out the analysis, the two main discrepancies between the two datasets,
151 namely regarding the spatial units (i.e. regions versus cells) and temporal frequency (year
152 versus dekad), must first be considered.

153 Given the focus of the study, the only fAPAR conditions that are relevant are the ones
154 observed over arable land. Therefore, the fAPAR anomaly data were first upscaled to NUTS 2
155 regions as a weighted average of all the 0.01° resolution fAPAR anomaly values within a
156 region, with a weighting factor based on the fraction of each grid-cell classified as arable land
157 according to the latest Corine land cover map (CLC2018, https://land.copernicus.eu/pan-

158 european/corine-land-cover/clc2018). This masking allows for removing from the NUTS 2
159 average all grid cells where the fAPAR dynamics are not related to agriculture (e.g. forest and
160 urban rural areas).

161   Regarding the temporal frequency, while fAPAR anomaly data are available throughout
162 the year, similar studies (e.g. Rojas et al., 2011) have focused only on data collected during
163 the growing season. A north-to-south gradient has been observed in the start, the end, and the
164 length of the growing season in Europe, with April-September being a common period all
165 over Europe, but with early start in February and late end in November over many areas
166 (Rötzer and Chmielewski, 2001). Estimations of the growing season directly based on
167 remotely sensed vegetation indices have also highlighted a very early start in the
168 Mediterranean, around October/November of the previous year (i.e. Atzberger et al., 2014),
169 likely related to combined effects (e.g. infesting weeds, early sowing and emergence) on the
170 remote sensing signal. Following these considerations, here we analyse an extended period,
171 testing the relationship between the yield of a particular year and the fAPAR anomalies
172 between the first dekad of October of the preceding year and the end of the current year, for a
173 total of 45 dekadal time series.

174   The set of correlation analyses between each of the 45 dekadal time series of fAPAR
175 anomalies and yearly yield data is used to construct a "correlogram", which relates the dekad
176 with the corresponding r value. The example of Tuscany region in Italy (Fig. 1) highlights
177 some common behaviours of the correlogram, such as a relative smooth transition between
178 periods of positive and negative r values. Different analyses can be performed, depending on
179 the critical values that are extracted from these plots and on the goal of the analysis. Here, we
180 faced the problem in two different ways: a) detecting periods of similar behaviour and
181 accuracy but variable length; and b) detecting periods of similar length but variable accuracy
182 and behaviour.

183   For these two analyses, we distinguished between two different behaviours in the
184 fAPAR-yield relationship, a direct relationship (i.e. negative anomalies in fAPAR correspond
185 to negative anomalies in yield) and an inverse relationship. The latter may occur when a
186 strong vegetative growth is observed early in the season during drought years, especially in
187 energy-limited conditions (van Hateren et al., 2021). We also distinguished between two
188 levels of accuracy, statistically significant correlations ($p < 0.05$, either positive or negative)
189 and a less stringent condition where at least different than zero r values (i.e. $|r| > 0.15$) are
190 considered. This second tier of values represent those conditions where a statistically
191 significant correlation (at $p < 0.05$) is not achieved, but a positive/negative relationship can

192   still be estimated. A value of 0.15 is used, as it corresponds to roughly 1/3 of r at $p = 0.05$ in
193   the case of a full sample.

194   By defining a period as a streak of consecutive dekads of length (L) between 2 and 45,
195   990 periods of various length can be analyzed for each region, and for each of these periods
196   four main metrics (ranging between 0 and 1) are computed: 1) F_{p+}, the fraction of r values in
197   the period that are positive and statistically significant (i.e. $r > 0$ and $p < 0.05$; 2) F_{p-}, the
198   fraction of r values in the period that are negative and statistically significant (i.e. $r < 0$ and p
199   < 0.05); 3) F_{+}, the fraction of r values in the period that are at least positive (i.e. $r > 0.15$), and
200   4) F_{-}, the fraction of r values in the period that are at least negative (i.e. $r < -0.15$). By
201   definition, F_{+} and F_{-} are always greater equal than F_{p+} and F_{p-}, respectively. We can then
202   focus on the longest periods (among the 990 periods) having homogeneous behaviour and
203   accuracy for a given region (homogeneous periods hereafter), e.g. a period with $F_{p+} = 1$. Due
204   to the smooth dynamics observed in most correlograms, these homogeneous periods are rather
205   well defined. In the rare instances when multiple homogeneous periods of the same length are
206   found for a region, the period closer to the surrounding regions is selected.

207   In the example reported in Figure 1, the dekads between 23 and 36 (light grey area) are
208   clearly part of the longest period with all positive and statistically significant r values, $L = 14$,
209   while the dark grey area demarks the longest period with $F_{-} = 1$ ($L = 6$).

210   A further set of analyses is focused instead on a fixed time window selected among a
211   limited range of lengths of the periods (i.e. a subset of periods among the 990 possible periods
212   with length from 2 to 45). The boundary values of this subset of periods can be derived from
213   the previous tests. Within these limits, an optimal positive (negative) period for each region
214   can be defined as the period with the maximum (minimum) average r value. Differently from
215   the first group of analyses, these optimal periods have varying F_{p+} and F_{+} (F_{p+} and F_{+}) values
216   (corresponding to the average r value) that can be used to quantify the robustness of the
217   relationship between fAPAR and yield. This analysis is performed on a subset of periods to
218   avoid selecting as optimal very short periods (i.e. of length 2) for regions with a prominent
219   peak value, or very long periods for regions where the correlogram is particularly flat.

220   Finally, while the analyses based on correlation give an insight on the relationship
221   between fAPAR and yield over the full spectrum of variability, a further test focused only on
222   extreme low yields is also performed, given that in the context of drought monitoring it would
223   be sufficient to be able to distinguish these conditions from the rest in order to successively
224   detect the drought-affected years. Here, the total number of cells for each region with fAPAR
225   anomalies < -1 (a common threshold used in extreme analyses) is computed during low yield

226 years (yield anomalies < -1), and it is compared with the same during the other years (yield
227 anomalies $\geq$ -1). The assumption of this analysis is that the ratio of these two quantities should
228 be greater than one in the case of a direct relationship.

229 **3. Results**

230 **3.1 Dynamics of yield anomalies and relationship with droughts**

231 While negative anomalies in yield can be often associated to drought events, the full dynamic
232 of standardized yield anomalies for cereals, as described in Section 2.1, cannot be exclusively
233 ascribed to the occurrence of drought conditions. However, the ability to capture the year-by-
234 year dynamics of yield using fAPAR anomalies is here evaluated with the goal of exploiting
235 this relationship in the framework of drought monitoring, hence the connection between low
236 yields and droughts need to be firstly assessed.

237 Figure 2 depicts the temporal evolution of yearly yield deviations, highlighting some
238 clear spatial patterns of significantly negative anomalies (i.e. yield anomaly < -1). Following a
239 review of the scientific literature for past drought events, it is possible to associate a
240 documented main drought event to many of these large clusters, as summarized in Table 1.
241 Seven main droughts are reported, ranging from the well-known drought in central Europe of
242 2003 (Rebetez et al., 2006) to the central-north European drought of 2018 (Buras et al., 2020;
243 Toreti et al., 2019).

244 The existence of a cause-effect relationship between these largest spatial patterns
245 observed in negative yield anomalies and the listed major drought events is further supported
246 by the study of Spinoni et al. (2015), which categorized the listed events (except the last two,
247 which occurred after that study) as being among the most severe in Europe according to
248 meteorological drought indices.

249 For each of the drought events listed in Table 1, specific independent scientific
250 references are also provided, which include details on the evolution of the meteorological
251 conditions, and the potential impacts on agriculture. Overall, analyses of these data tend to
252 support that the adopted dataset of yield anomalies shows the impacts on vegetation of the
253 major European droughts, in conformance with the conclusions of other studies at regional
254 level in Europe (Bachmair et al., 2018; Potopová et al., 2015), or for other parts of the world
255 (e.g. Yang et al., 2020).

256 **3.2 Detection of the homogeneous periods in the fAPAR-yield relationship**

257   While many studies focused on the local maximum r value to detect when and where
258 fAPAR and annual yield anomalies best correlate, isolated peak values may alter the
259 perception of the robustness of fAPAR as a proxy variable of yield. In the context of an
260 operational drought monitoring system, where continuous estimates should be provided rather
261 than "one shot" predictions, information on longer homogeneous time periods are more
262 valuable.

263   Focusing first on the positive r values, we analysed the periods with only statistically
264 significant values ($F_{p+} = 1$), or only at least positive values ($F_+ = 1$). The maps in Figure 3
265 reports the local maximum lengths corresponding to these two quantities, namely positive
266 homogeneous periods. Both of these maps show generally longer homogeneous periods in
267 southern Europe, with the largest values observed for some Mediterranean regions (e.g. most
268 of Spain, Cyprus, Sicily, Apulia and the Aegean/Mediterranean Turkey), and the smallest
269 values (or no homogeneous period at all) mostly located in Central Europe (i.e. Germany,
270 Poland and north-eastern France). On average, the maximum length of the periods with F_{p+}
271 =1 is limited in most of the cases (5.5 ± 4.3 dek, almost 2 months), whereas the values more
272 than double in the case of $F_+ = 1$ (13.0 ± 8.3 dek, more than 4 months).

273   Generally, almost all the maximum r values in the correlograms are obtained in the
274 dekads between mid-February and mid-September, which is expected since this period aligns
275 well with what is commonly considered the growing season in Europe (Atzberger et al., 2014;
276 Rötzer and Chmielewski, 2001). Nonetheless, a large variability in the length of both positive
277 homogeneous periods is observed, with southern and central Europe confirmed to be not only
278 the areas with highest and lowest r values, respectively, but also the areas with the longest (i.e.
279 4-7 months) and shortest (up to 2 months) periods with consecutive statistically significant
280 positive correlations.

281   Due to the large variability in the length of the homogeneous periods observed in Figure
282 3, a direct analysis of the spatial patterns in the starting and ending dekads is not feasible. So,
283 in order to evaluate synthetically the temporal location of these homogeneous periods, we
284 analyzed which dekads each of them covers, and computed for every dekad the fraction of
285 NUTS 2 regions (out of 240) that includes that particular dekad in the homogeneous period
286 (Fig. 4). For example, dekad 27 (i.e. the first dekad of July starting from the beginning of
287 October of the previous year) is part of the maximum homogeneous period in about 20% and
288 50% of the regions, for F_{p+} and F_+, respectively. It is worth noting that about 21% of the
289 NUTS 2 regions do not have a period (minimum 2 consecutive dekads) with $F_{p+} = 1$.

290   It is possible to observe two "flexing points" in each of the two time series in Figure 4
291   around 0.1 for F_{p+} and 0.2 for F_+. Starting from these values, we can detect two optimal
292   homogeneous periods: from end-of-April to mid-October (6 months) for F_{p+}, and from March
293   to early-November (8 months) for F_+.

294   Moving to the negative correlation values, two maps analogous to the ones in Figure 3
295   are reported in Figure 5 for F_{p-} (panel a) and F_- (panel b). These two maps show how the
296   longest negative homogeneous periods are in general shorter than the ones for positive
297   correlations, with an average value of 3.0 ± 1.6 dekads for F_{p-} and 7.0 ± 3.9 for F_-. The lack of
298   statistically significant negative r values is especially evident, with almost 50% of the regions
299   having no homogeneous periods with $F_{p-} = 1$. The map for F_- (Fig. 5b) allows for some
300   additional considerations on the spatial distribution, with moderate maximum lengths (around
301   9 dekads) in most of western and central Europe, and some high values (higher than 15
302   dekads) in some regions of southern Europe.

303   In terms of temporal distribution, the histograms on Figure 6 depict the fraction of
304   NUTS 2 regions that includes that particular dekad in the negative homogeneous periods.
305   Overall, the fraction values are lower than the ones observed for the positive periods (see Fig.
306   4), with two distinguishable peak periods in the F_- values, the first in early season (February-
307   May) and the second after the end of the season (October-December, sowing period for the
308   winter crops).

309   Most of the homogeneous periods early in the season correspond to regions in western
310   and southern Europe, and the late season periods are mostly located in central and northern
311   Europe. In the framework of drought monitoring, the first can be potentially exploited as early
312   warning signals of subsequent reduction in fAPAR due to drought (as seen in the positive
313   homogenous periods that usually follows in the correlograms). The second mostly occur right
314   after the harvesting season, and hence as no value for early warning systems.

315   **3.3 Performance for a fixed time-window**

316   A clear outcome of the previous analyses is that the length of the homogeneous periods
317   with negative correlations is limited compared to the positive correlations, and mostly useful
318   for drought monitoring only early in the growing season. Therefore, we focus only on the
319   positive correlation values for the successive analyses. The two lengths (6 and 8 months)
320   derived from the data depicted in Fig. 4 are used as the minimum and maximum boundary
321   values to find the local optimal period for each region (see Section 2.3).

322   The results of this bounded analysis of the local optimal period are shown in Fig. 7,
323   where the starting dekad (d_i, panel a) and ending dekad (d_e, panel b) of the optimal period are
324   depicted for every region. Fig. 7a shows a general pattern of an early start in Central Europe
325   (i.e. February/March), and in few southern regions of the Mediterranean, and a late start (i.e.
326   May/June) in most of southern and western Europe. This late start is of course in line with the
327   previously observed negative correlations in February/May over the same regions.
328   Analogously, Fig. 7b shows that the end of the optimal period occurs mostly around
329   October/November, after the harvesting, in both southern and western Europe, and
330   August/September in central Europe, with then mostly negative correlations in central and
331   north Europe occurring after this period (likely due to spurious correlations).

332   Given that these optimal periods have been derived based on the average r values in the
333   6 to 8-month period, the F_{p+} and F_+ values corresponding to these optimal periods can assume
334   any values between 0 and 1 (no significant/positive r values to all significant/positive r values
335   within the optimal periods). For this reason, we classified each region based on the combined
336   values of these two metrics, as represented by the legend included in Fig. 8. In this map, the
337   green areas show a good capability to reproduce the dynamic of yield deviation for the whole
338   optimal period (the fraction of high r values in the two optimal periods is high), with the
339   regions in dark green having the overall best performance (over half of dekads with
340   statistically significant r values and more than 2/3 with at least positive values). Conversely,
341   the red regions show a poor capability of the fAPAR anomalies to capture the yield dynamics,
342   with the dark red regions having less than 1/10 of statistically significant values (i.e. less than
343   a month) and less than 1/3 of positive correlations during the optimal period.

344   Overall, slightly more than half (i.e. 55.8%) of the study regions are classified in one of
345   the green classes, with a predominance of these regions in Mediterranean and south-eastern
346   Europe. The rest of the study area is almost equally split between regions with average
347   performance (yellow class, 23.3%), and poor performance (red classes, 20.9%). Among the
348   red classes, the majority of the regions fall in the category with intermediate F_+ values ($1/3 <$
349    $F_+ < 2/3$) but low statistically significance ($F_{p+} < 1/10$). Most of these regions are located in
350   central Europe, between northern France, the United Kingdom, Germany and Poland.

351   Spain stands out as having particularly robust performances, even among the generally
352   good performing Mediterranean area. While the start and end of the optimal period varies
353   across the area (March to May, and September to November, respectively), the results are
354   consistently in the best class (dark green in Fig. 8). Among the Mediterranean countries, some
355   mixed results can be observed in Italy and Greece.

3.4 Detection of low yield years

The previous analyses show a noticeable difference in the performance of fAPAR anomalies to capture the full range of variability of yield anomalies across Europe, as quantified by the results on the optimal periods summarize in Figure 8. For the same optimal periods, the number of fAPAR anomalies < -1 were cumulated for low yield years (yield anomaly < -1) and the other years, separately, and the ratio between these two quantities is depicted in Figure 9.

Overall, values greater than 1 are observed over most of Europe in Figure 9, suggesting a good performance of fAPAR anomalies to detect extreme low conditions in annual yield. While the ratio is only slightly higher than one in some regions where the previous analyses highlight poor performances (i.e. the UK and France), years with severe reductions in yield are still well-captured by fAPAR.

Finally, the plot in Figure 10 shows a comparison between the ratio computed on the optimal period (grey area) and the one computed on the full year (all 36 dekads, black area). Since the years are divided in the two categories based on yield data, the size of the two datasets is independent from the selected period (optimal or full year), making the intercomparison straightforward. The plot show an overall increase in the ratio when only the dekads in the optimal period are considered, which translate in a better ability to discriminate low yield years compared to simply account for all the anomalies observed across the full year.

4. Discussion

The value of the results reported in the previous section in the context of drought monitoring is related to the assumption that anomalies of cereal yields show the effects of drought on vegetation during drought years, as demonstrated for example by Brás et al. (2021) who quantified an approximately 9% reduction in European cereal yields due to historical droughts (1961-2018), with an increasing intensity in more recent years. The spatial patterns in negative yield anomalies for the dataset used in this study, and the cross comparison with documented past drought events, confirm the general assumption that low yields are recorded during drought years, even if not all the low yield values may be associated to droughts. These data confirm that understanding the role of fAPAR as proxy of yield is valuable for drought monitoring, even if a non exclusive correspondence between low yield/fAPAR and drought exists.

Eliminato: h

388   Due to the focus on data commonly used in operational drought monitoring systems, a
389   common element for all the performed analyses is the independent use of each dekadal
390   fAPAR time series. While different results may be achieved by using metrics based on the full
391   growing season (e.g. Kang et al., 2018), such analyses are not easily transferable to a near-real
392   time monitoring framework. Overall, the correlation coefficients computed using fAPAR
393   collected during multiple dekads suggests a predominance of positive values over all regions.
394   This is in line with the expected direct relationship between fAPAR and yield during the core
395   growing season, as well as with most of the past studies which focused primarily on the
396   positive correlation. Indeed, most of the maximum values of correlation seems to be located
397   within the conventional growing season, and the south-north gradient observed in both of the
398   positive homogeneous period maps (Fig. 3) is in broad agreement with the expected
399   increasing gradient in growing season length observed over Europe (Rötzer and Chmielewski,
400   2001). However, there is not a perfect matching between the growing seasons and the periods
401   with higher correlation values, and while studies on satellite-derived phenology have detected
402   growing season lengths ranging from 5 to 9 months (Rötzer and Chmielewski, 2001), the
403   average length of the periods with positive and statistically significant correlations seems to
404   be shorter.

405   Consistently high positive correlation values are obtained over most of Spain, in line
406   with a recent study over the region (García-León et al., 2019), which reported good
407   performances of the satellite-based Vegetation Condition Index (VCI) for different type of
408   cereals, especially for winter wheat and barley. Over central Italy, Todisco et al. (2008)
409   observed good correlation between yield in sunflower and sorghum with common drought
410   indices (Standardized Precipitation Index, SPI, and Soil Moisture Severity Index), with a
411   maximum correlation around weeks 27-29 of the growing season (i.e. July) and statistically
412   significant values for periods ranging from 2 to 4 months. Similar timing, but with a slightly
413   shorter optimal length, has been observed in our analysis for the same area.

414   For Germany, Bachmair et al. (2018) found significant correlation values between VCI
415   and Vegetation Health Index (VHI) anomalies in the month of August, and yield deviations
416   for maize, that are comparable with the maximum values observed for western Germany in
417   our study. A mix of high correlation and missing data is reported in that study for eastern
418   Germany, where our results are statistically significant only for a very limited period. These
419   differences may be explained by the focus on specific crop types (not included in our study),
420   as the same authors also highlight how the accuracy of their relationships varied for the
421   different crops.

422   Similar to our results, Labudová et al. (2017) found significant correlation with SPI and
423   Standardized Precipitation Evapotranspiration Index (SPEI) in the Danubian lowlands only
424   for summer months, or for a very limited time (i.e. June) in the Eastern Slovak lowlands. For
425   these regions, the values of the maximum homogeneous period with F_{p+} =1 ranged between 3
426   and 9 dekads as shown in Fig. 3.

427   The good results observed over the western Mediterranean and the countries around the
428   Black Sea are in agreement with the founding of López-Lozano et al. (2015), which reported a
429   similar pattern in their study based on a different fAPAR product (derived from SPOT-VGT
430   data). This seems to suggest that the observed relationship are likely independent from the
431   data source, and more intrinsically connected to the capability of the physical quantity
432   fAPAR to reflect the variation in yield under certain conditions.

433   The presence of limited periods with consecutive negative correlations early in the
434   growing season may be related to the lagged response of vegetation to water deficits (Crow et
435   al., 2012), which results in positive greenness anomalies early in the season followed by
436   negative values later on (i.e. delay in the phenological cycle). Another explanation can be the
437   limited immediate effect of water deficit during energy-limited periods (Zscheischler et al.,
438   2015), which can also be the reason behind the general poor correlation between fAPAR and
439   yield over regions where water is not a key limiting factor. This inverse relationship observed
440   early in the season is currently under-explored in drought monitoring systems, which mostly
441   focus on the direct relationship, and it may have an interesting role as an early warning tool
442   under specific conditions. However, the results obtained in this study suggest a limited
443   temporal extension and statistical robustness of the periods with inverse relationships, which
444   usually are followed by much longer and robust periods of direct relationship.

445   The late start of the optimal period in many regions of the Mediterranean and western
446   Europe, compared to the rest of the domain, is associate to the presence of these periods of
447   inverse relationship early in the growing season. Given the particular climate of the
448   Mediterranean region, and the key role of dry and hot spring-summer months in propagating
449   the water deficits in the area, a lagged response in vegetation is expected. In contrast, Central
450   Europe is characterized by an earlier start of the optimal period (March to August), compared
451   to the Mediterranean and western Europe, that seems to precede the expected growing season
452   (June to October), further stressing the imperfect match between optimal period and growing
453   season. For central Europe, Potopová et al. (2015) found high yield-drought correlation for
454   cereals (better than other crops) over Czech Republic between April-June, a result in line with
455   our findings. The late start (April/May) in the northern regions of Scandinavia compared to

456 central Europe, is mostly explained by the lack of reliable fAPAR data earlier in the year, due
457 to low sun angles.

458 Focusing on the optimal period, mixed performances are obtained in Italy, with low
459 agreement particularly in Sardinia and regions along the Apennine mountains. Although
460 García-León et al. (2021) found a positive relationship between annual-cumulated fAPAR
461 anomalies and yield for most main crop types, the aggregation of the results at national scale
462 does not allow the detection of differences among regions. Given the complex morphology of
463 those regions, potential unreliability in the fAPAR estimates may be a possible cause for the
464 poor performances. Complex morphology can also be the reason for poor results over few
465 other Mediterranean areas, such as Greece.

466 The spatial variability of the dependence of yield to water-limiting factors can be one of
467 the explanation of the observed patterns, with stronger correlation between fAPAR and yield
468 over water-limited regions (Zampieri et al. 2017), and weaker relationships over regions
469 where other factors may play a major role in controlling yield rather than simply greenness
470 dynamics. Similar considerations were also made by López-Lozano et al. (2015), even when
471 results are disentangle between different crop types (wheat, barley and maize).

472 Indeed, another possible contributing factor underlying the spatial differences in the
473 retrieved optimal periods can be the potentially variable response of different cereal types
474 included within the overall cereals Eurostat category. Since different predominant cereal types
475 are cultivated locally, this variability can also contribute to the observed spatial variability in
476 the results. This is supported by other studies that have demonstrated different responses for
477 different crop types (García-León et al., 2021; Labudová et al., 2017). While applying the
478 analysis to different cereals sub-categories, or even different plant types, may be useful to
479 understand better the relationship between fAPAR and yield for each specific crop, the results
480 of this study for all cereals provide valuable experimental information on optimal periods that
481 can be more easily integrated into an operational drought monitoring system, which does not
482 only focus on agricultural drought impacts.

483

484

485 **5. Summary and Conclusions**

486 In this study, records of annual crop yield data for cereals were used to evaluate the
487 performance of satellite-derived fAPAR time series data in capturing year-by-year variations
488 in crop production for different periods of the year and growth stages of vegetation, given that

489   fAPAR anomalies (or other greenness indices) are often used in drought studies to capture the
490   effect of drought events on vegetation in absence of yield data.

491   Overall, the analysis of the correlograms computed by plotting anomalies of dekadal
492   fAPAR values against yearly yield deviations, was used for three main purposes:

493   ▪ Investigation on continuous streaks of dekads with homogeneous behaviour (direct *vs.*
494   inverse) and agreement (i.e. statistical significance) but with different temporal length.
495   ▪ Investigation of fixed length (6 to 8 months) optimal periods, defined as function of
496   the maximum average *r* within the given range of lengths.
497   ▪ Evaluation of the capability of fAPAR anomalies during the optimal periods to
498   discriminate between low yield and other years.

499   The analyses confirm the period March to October as being the most relevant to
500   positively correlate anomalies of fAPAR and crop yield, being the period when most of the
501   highest values of correlation are estimated, and when most of the continuous periods with
502   statistically significant and positive *r* values are located. There is a generally good agreement
503   between these findings an both the duration and temporal location of the commonly defined
504   growing seasons in Europe, even if spatial patterns in periods with positive correlations and
505   growing season can also be rather different. While some periods with consistent negative
506   correlations are also observed between February and May, these are generally limited in
507   length to be considered as primary source of information to reproduce yield dynamics, but
508   they have potential as valuable early warning information.

509   The average growing period in Europe is usually characterized by a marked south-to-
510   north gradient, which is also observed in our analysis of the 6- to 8-month optimal periods
511   based on average *r* values. Some clear spatial patterns emerge in this analysis, such as the
512   early start in most of central Europe and the southern Mediterranean, and the late start in
513   southern and western Europe. These spatial patterns do not exactly match commonly observed
514   satellite-derived growing seasons, so they provide an independent assessment of which phases
515   of the phenological cycle are more valuable to capture yield variations, a valuable information
516   that can be incorporated into operational drought monitoring systems.

517   Another key output of the study is the generally good correlation between fAPAR
518   anomalies and crop yield anomalies over most of the Mediterranean regions and across the
519   full range of variability of yield data. This result can be explained by the strong dependency
520   of both yield and vegetation greenness to water-limiting factors, as also suggested by López-
521   Lozano et al. (2015) and Zampieri et al. (2017). Given the well documented high vulnerability
522   of this region to drought and the increasing threat posed by climate change (Cammalleri et al.,

523   2020; Dubrovský et al., 2014), this result suggests the possibility to link satellite-observed
524   fAPAR anomalies with actual impacts in agriculture, as a promising new development that
525   merits further exploration.

526   This study also highlighted the overall limited correlation, outside of very short time
527   periods, between fAPAR and yield over most of the NUTS 2 regions in central Europe.
528   Further analyses may be needed to better understand the reason behind this result. In this
529   context, a recent study by Beillouin et al. (2020) has demonstrated how simple climate
530   variables (i.e. high temperature and low precipitation) can explain much of the yield
531   variability in central Europe, in contrast with the situation in southern Europe. It is important
532   to further remark that even over these regions where the overall performance is limited,
533   fAPAR anomalies are still successful in discriminating between low yield years and the rest,
534   which is still a relevant feature to be further exploited in drought monitoring systems.

535

536

537   **Data availability:** The fAPAR dataset used in this study can be retrieved from the JRC Data
538   catalogue (EDO, 2021).

539

540   **Author contribution:** CC designed the experiments with inputs from AT and NMC. CC
541   developed the codes and performed the analyses. CC prepared the manuscript with
542   contributions and revisions from all co-authors.

543

544   **Competing interests:** The authors declare that they have no conflict of interest.

References

Atzberger, C., Klisch, A., Mattiuzzi, M., and Vuolo, F.: Phenological metrics derived over the European continent from NDVI3g data and MODIS time series, Remote Sens., 6(1), 257-284, https://doi.org/10.3390/rs6010257, 2014.

Bachmair, S., Tanguy, M., Hannaford, J. and Stahl, K.: How well do meteorological indicators represent agricultural and forest drought across Europe?, Env. Res. Letters, 13, 034042, https://doi.org/10.1088/1748-9326/aaafda, 2018.

Barros, J.R.A., Guimaraes, M.J.M., Simões, W.L., de Melo, N.F. and Angelotti, F.: Water restriction in different phenological stages and increased temperature affect cowpea production, Agr. Sci., 45, 1-12, https://doi.org/10.1590/1413-7054202145022120, 2021.

Beillouin, D., Schauberger, B., Bastos, A., Ciais, P. and Makowski, D.: Impact of extreme weather conditions on European crop production in 2018, Phil. Trans. R. Soc. B, 375, 20190510, https://doi.org/10.1098/rstb.2019.0510, 2020.

Bogdan, O., Marinică, I. and Mic, L.-E.: Characteristics of the summer drought 2007 in Romania, Proceedings of the 2008 BALWOIS Conference, 27-31 May 2008, Ohrid, Republic of Macedonia. Available at: http://balwois.com/wp-content/uploads/old_proc/ffp-1075.pdf, 2008. [last access: July 2021].

Brás, T.A., Seixas, J., Carvalhais, N. and Jägermeyr, J.: Severity of drought and heatwave crop losses tripled over the last five decades in Europe, Environ. Res. Lett., 16, 065012, https://doi.org/10.1088/1748-9326/abf004, 2021.

Brown, R.G. and Meyer, R.F.: The fundamental theory of exponential smoothing, Oper. Res., 9, 673-685, https://doi.org/10.1287/opre.9.5.673, 1961.

Buras, A., Rammig, A. and Zang, C.S.: Quantifying impacts of the drought 2018 on European ecosystems in comparison to 2003, Biogeosciences, 17, 1655-1672, https://doi.org/10.5194/bg-17-1655-2020, 2020.

Cammalleri, C., Naumann, G., Mentaschi L., Bisselink, B., Gelati, E., de Roo, A. and Feyen, L.: Diverging hydrological drought traits over Europe with global warming, Hydrol. Earth Syst. Sci., 24, 5919-5935, https://doi.org/10.5194/hess-24-5919-2020, 2020.

Ceglar, A., Toreti, A., Zampieri, M., Manstretta, V., Bettati, T. and Bratu, M.: Clisagri: An R package for agro-climate services, Climate Serv., 20, 100197, https://doi.org/10.1016/j.cliser.2020.100197, 2020.

Chaves, M.M., Pereira, J.S., Maroco, J., Rodrigues, M.L., Ricardo, C.P.P., Osório, M.L., Carvalho, I., Faria, T. and Pinheiro, C.: How Plants Cope with Water Stress in the

578   Field?, Photosynthesis and Growth. Annals Botany, 89(7), 907-916,
579   https://doi.org/10.1093/aob/mcf105, 2002.

580   Crow, W., Kumar, S.W. and Bolten, J.D.: On the utility of land surface models for
581   agricultural drought monitoring, Hydrol. Earth Syst. Sci., 16, 34-51-3460,
582   https://doi.org/10.5194/hess-16-3451-2012, 2012.

583   De Bono, A., et al. & United Nations Environment Programme: Impacts of Summer 2003
584   Heat Wave in Europe, Environment Alert Bulletin, vol. 2, p. 4. Available at:
585   http://archive-ouverte.unige.ch/unige:32255 [last access: September 2022], 2004.

586   Demuth, S.: Learning to live with drought in Europe, A World of Science, 7(3), 18–20.
587   Available at: https://www.geo.uio.no/edc/downloads/ [last access: October 2022], 2009.

588   Demirevska, K., Zasheva, D., Dimitrov, R., Simova-Stoilova, L., Stamenova, M. and Feller,
589   U.: Drought stress effects on Rubisco in wheat: changes in the Rubisco large subunit,
590   Acta Phisiol. Plant, 31, 1129-1138, https://doi.org/10.1007/s11738-009-0331-2, 2009.

591   Dubrovský, M., Hayes, M., Duce, P., Trnka, M., Svoboda, M. and Zara, P.: Multi-GCM
592   projections of future drought and climate variability indicators for the Mediterranean
593   region, Reg. Environ. Change, 14, 1907-1919, https://doi.org/10.1007/s10113-013-
594   0562-z, 2014.

595   European Drought Observatory, EDO: EDO Fraction of Absorbed Photosynthetically Active
596   Radiation (FAPAR) Anomaly (MODIS) (version 1.3.2), European Commission, Joint
597   Research Centre (JRC) [Dataset] PID: http://data.europa.eu/89h/91a222a0-74fe-468f-
598   b53a-b622aa1161cf, 2021.

599   Eurostat: Annual crop statistics: Handbook 2020 edition, 167 pp. Available at:
600   https://ec.europa.eu/eurostat/cache/metadata/Annexes/apro_cp_esms_an1.pdf   [last
601   access: July 2021], 2020.

602   Food and Agriculture Organization of the United Nations (FAO): The impact of natural
603   hazards and disasters on agriculture and food security and nutrition: A call for action to
604   build resilient livelihoods, Rome, Italy, 16 pp. Available at:
605   http://www.fao.org/3/i4434e/i4434e.pdf [last access: July 2021], 2015.

606   Food and Agriculture Organization of the United Nations (FAO), International Fund for
607   Agricultural Development (IFAD), United Nations Children's Fund (UNICEF) and
608   World Food Programme (WFP), World Health Organization (WHO): The State of Food
609   Security and Nutrition in the World 2018, Building climate resilience for food security
610   and nutrition, Rome, Italy, 202 pp. Available at:
611   https://www.fao.org/3/I9553EN/i9553en.pdf [last access: December 2021], 2018.

612 Food and Agriculture Organization of the United Nations (FAO): The impact of disasters and
613   crises on agriculture and food security: 2021, Rome, Italy, 245 pp. Available at:
614   https://doi.org/10.4060/cb3673en [last access: September 2022], 2021.

615 García-Herrera, R., Paredes, D., Trigo, R.M., Trigo, I.F., Hernandez, H., Barriopedro, D. And
616   Mendes, M.T.: The outstanding 2004-2005 drought in the Iberian Peninsula: associated
617   atmospheric circulation, J. Hydrometeorol., 8, 483–498,
618   https://doi.org/10.1175/JHM578.1, 2007.

619 García-Herrera, R., Garrido-Perez, J.M., Barriopedro, D., Ordóñez, C., Vicente-Serrano,
620   S.M., Nieto, R., Gimeno, L., Sorí, R. and Yiou, P.: The European 2016/17 Drought, J.
621   Climate, 32, 3169-3187, https://doi.org/10.1175/JCLI-D-18-0331.1, 2019.

622 García-León, D., Contreras, S. and Hunink, J.: Comparison of meteorological and satellite-
623   based indices as yield predictors of Spanish cereals, Agr. Water Manage., 213, 388-396,
624   https://doi.org/10.1016/j.agwat.2018.10.030, 2019.

625 García-León, D., Standardi, G. and Staccione, A.: An integrated approach for the estimation
626   of agricultural drought costs, Land Use Policy, 100, 104923,
627   https://doi.org/10.1016/j.landusepol.2020.104923, 2021.

628 Gouveia, C., Trigo, R.M. and DaCamara, C.C.: Drought and vegetation stress monitoring in
629   Portugal using satellite data, Nat. Hazards Earth Syst. Sci., 9, 185-195,
630   https://doi.org/10.5194/nhess-9-185-2009, 2009.

631 Kang W., Wang, T. and Liu, S.: The response of vegetation phenology and productivity to
632   drought in semi-arid regions of northern China, Remote Sens., 10(5), 727,
633   https://doi.org/10.3390/rs10050727, 2018.

634 Knyazikhin, Y., Martonchik, Y.V., Myneni, R.B., Diner, D.J. and Running, S.W.: Synergistic
635   algorithm for estimating vegetation canopy leaf area index and fraction of absorbed
636   photosynthetically active radiation from MODIS and MISR Data, J. Geophys. Res.,
637   103, 32257–32274, doi:10.1029/98JD02462, 1998.

638 Klisch, A. and Atzberger, C.: Evaluating phenological metrics derived from the MODIS time
639   series over the European continent, PFG, 5, 409-421, https://doi.org/10.1127/1432-
640   8364/2014/0233, 2014.

641 Labudová, L., Labuda, M. and Takáč, J.: Comparison of SPI and SPEI applicability for
642   drought impact assessment on crop production in the Danubian lowland and the East
643   Slovakian lowland, Theor. Appl. Climatol., 128, 491-506,
644   https://doi.org/10.1007/s00704-016-1870-2, 2017.

645 López-Lozano, R., Duveiller, G., Seguini, L., Meroni, M., García-Condado, S., Hooker, J.,
646   Leo, O. and Baruth, B.: Towards regional grain yield forecasting with 1km-resolution
647   EO biophysical products: Strengths and limitations at pan-European level, Agric. Forest
648   Meteorol., 206, 12–32, https://doi.org/10.1016/j.agrformet.2015.02.021, 2015.

649 Monteleone, B., Borzí, I., Bonaccorso, B. and Martina, M.: Developing stage-specific drought
650   vulnerability curves for maize: The case study of the Po River basin, Agric. Water
651   Manag., 269(C), 107713, https://doi.org/10.1016/j.agwat.2022.107713, 2022.

652 Myneni, R.B.: MOD15A2H MODIS/Terra Leaf Area Index/FPAR 8-Day L4 Global 500m
653   SIN   Grid   V006.   NASA   EOSDIS   Land   Processes   DAAC,
654   https://doi.org/10.5067/modis/mod15a2h.006, 2015.

655 Potopová, V., Štepánek, P., Možný, M., Turoktt, L. and Soukup, J.: Performance of the
656   standardized precipitation evapotranspiration index at various lags for agricultural
657   drought risk assessment in the Czech Republic, Agric. For. Meteorol., 202, 26-38,
658   https://doi.org/10.1016/j.agrformet.2014.11.022, 2015.

659 Rebetez, M., Mayer, H., Dupont, O., Schindler, D., Gartner, K., Kropp, J.P. and Menzel, A.:
660   Heat and drought 2003 in Europe: A climate synthesis, Ann. For. Sci., 63, 569-577,
661   https://doi.org/10.1051/forest:2006043, 2006.

662 Rembold, F., Meroni, M., Urbano, F., Csak, G., Kerdiles, H., Perez-Hoyos, A., Lemoine, G.,
663   Leo, O. and Negre, T.: ASAP: A new global early warning system to detect anomaly
664   hot spots of agricultural production for food security analysis, Agr. Systems, 168, 247-
665   257, https://doi.org/10.1016/j.agsy.2018.07.002, 2019.

666 Rojas, O., Vrieling, A. and Rembold, F.: Assessing drought probability for agricultural areas
667   in Africa with coarse resolution remote sensing imagery, Remote Sens. Environ., 115,
668   343-352, https://doi.org/10.1016/j.rse.2010.09.006, 2011.

669 Rossi, S., Weissteiner, C., Laguardia, G., Kurnik, B., Robustelli, M., Niemeyer, S. and
670   Gobron, N.: Potential of MERIS fAPAR for drought detection. In: Proceedings of the
671   2nd MERIS/(A)ATSR User Workshop, ESA SP-666, edited by H. Lacoste and L.
672   Ouwehand, 6. Frascati, Italy, ESA Communication production Office, 2008.

673 Rötzer, T. and Chmielewski, F.M.: Phenological maps of Europe, Climate Res., 18, 249-257,
674   https://doi.org/10.3354/cr018249, 2001.

675 Sassenrath, G.F., Schneider, J.M., Gaj, R., Grzebisz, W. and Halloran, J.M.: Nitrogen balance
676   as an indicator of environmental impact: Toward sustainable agricultural production,
677   Renew.   Agric.   Food   Syst.,   28(3),   276-289,
678   https://doi.org/10.1017/S1742170512000166, 2012.

679   Sima, M., Popovici, E.-A., Bălteanu, D., Micu, D.A., Kucsicsa, G., Dragotă, C. and
680   Grigorescu, I.: A farmer-based analysis of climate change adaptation options of
681   agriculture in the Bărăgan Plain, Romania, Earth Perspect., 2, 5,
682   https://doi.org/10.1186/s40322-015-0031-6, 2015.

683   Somorowska, U.: Changes in drought conditions in Poland over the past 60 years evaluated
684   by the Standardized Precipitation-Evapotranspiration Index, Acta Geophys., 64(6), 25-
685   30-2549, https://doi.org/10.1515/acgeo-2016-0110, 2016.

686   Spinoni, J., Naumann, G., Vogt, J.V. and Barbosa, P.: The biggest drought events in Europe
687   from 1950 to 2012, J. Hydrol. Reg. Studies, 3, 509-524,
688   https://doi.org/10.1016/j.ejrh.2015.01.001, 2015.

689   Stahl, K., Kohn, I., Blauhut, V., Urquijo, J., De Stefano, L., Acácio, V., Dias, S., Stagge, J.H.,
690   Tallaksen, L.M., Kampragou, E., Van Loon, A.F., Barker, L.J., Melsen, L.A., Bifulco,
691   C., Musolino, D., de Carli, A., Massarutto, A., Assimacopoulos, D. and Van Lanen,
692   H.A.J.: Impacts of European drought events: insights from an international database of
693   text-based reports, Nat. Hazards Earth Syst. Sci., 16, 801-819,
694   https://doi.org/10.5194/nhess-16-801-2016, 2016.

695   Stallmann, J., Schweiger, R., Pons, C.A.A. and Müller, C.: Wheat growth, applied water use
696   efficiency and flag leaf metabolome under continuous and pulsed deficit irrigation, Sci.
697   Rep., 10, 10112, https://doi.org/10.1038/s41598-020-66812-1, 2020.

698   Tadesse T., Senay, G.B., Berhan, G., Regassa, T. and Beyene, S.: Evaluating a satellite-based
699   seasonal evapotranspiration product and identifying its relationship with other satellite-
700   derived products and crop yield: a case study for Ethiopia, Int. J. Appl. Earth Obs.
701   Geoinf., 40, 39-54, https://doi.org/10.1016/j.jag.2015.03.006, 2015.

702   Todisco, F., Vergni, L. and Mannocchi, F.: An evaluation of some drought indices in the
703   monitoring and prediction of agricultural drought impact in central Italy, in: Santini A.,
704   Lamaddalena N., Severino G., Palladino M. (eds.), Irrigation in Mediterranean
705   agriculture: challenges and innovation for the next decades, Bari : CIHEAM, 2008, 203-
706   211, Options Méditerranéennes: Série A, Séminaires Méditerranéens; n. 84. Available
707   at: http://om.ciheam.org/article.php?IDPDF=800967 [last access: July 2021], 2008.

708   Toreti, A., Belward, A., Perez-Dominguez, I., Naumann, G., Luterbacher, J., Cronie, O.,
709   Seguini, L., Manfron, G., Lopez-Lozano, R., Baruth, B., van den Berg, M., Dentener,
710   F., Ceglar, A., Chatzopoulos, T. and Zampieri, M.: The Exceptional 2018 European
711   Water Seesaw Calls for Action on Adaptation, Earth's Future, 7(6), 652-663,
712   https://doi.org/ 10.1029/2019EF001170, 2018.

713 United Nations Office for Disaster Risk Reduction: GAR Special Report on Drought 2021,
714   Geneva, 210 pp. ISBN: 9789212320274. Available at:
715   https://www.undrr.org/publication/gar-special-report-drought-2021 [last access: July
716   2021], 2021.

717 Valiukas, D.: Analysis of droughts and dry periods in Lithuania. Summary of Doctoral
718   Dissertation, Vilnius University, 49 pp. Available at:
719   https://epublications.vu.lt/object/elaba:8754330 [last access: July 2021], 2015.

720 van Hateren, T.C., Chini, M., Matgen, P. and Teuling, A.J.: Ambiguous agricultural drought:
721   Characterising soil moisture and vegetation droughts in Europe from earth observation,
722   Remote Sens., 13(19), 1990, https://doi.org/10.3390/rs13101990, 2021.

723 Vicente-Serrano, S.M., Beguería, S., Lorenzo-Lacruz, J., Camarero, J.J., López-Moreno, J.I.,
724   Azorin-Molina, C., Revuelto, J., Morán-Tejeda, E. and Sanchez-Lorenzo, A.:
725   Performance of drought indices for ecological, agricultural, and hydrological
726   applications, Earth Interact., 16, 1-27, doi:10.1175/2012EI000434.1, 2012.

727 Wang, Y., Tian, Y., Zhang, Y., El-Saleous, N., Knyazikhin, Y., Vermote, E., and Myneni,
728   R.B.: Investigation of product accuracy as a function of input and model uncertainties:
729   Case study with SeaWiFS and MODIS LAI/FPAR algorithm, Remote Sens. Environ.,
730   78, 296-311, doi:10.1016/S0034-4257(01)00225-5, 2001.

731 World Meteorological Organization (WMO) and Global Water Partnership (GWP):
732   Handbook of Drought Indicators and Indices (M. Svoboda and B.A. Fuchs), Integrated
733   Drought Management Programme (IDMP), Integrated Drought Management Tools and
734   Guidelines Series 2, Geneva, 53 pp, 2016.

735 Yang, J., Wu, J., Liu, L., Zhou, H., Gong, A., Han, X. and Zhao, W.: Response of winter
736   wheat to drought in the north China plain: spatial-temporal patterns and climate drivers,
737   Water, 12, 3094, https://doi.org/10.3390/w12113094, 2020.

738 Zampieri, M., Ceglar, A., Dentener, F. and Toreti, A.: Wheat yield loss attributable to heat
739   waves, drought and water excess at the global, national and subnational scales, Env.
740   Res. Lett., 12(6), 064008, https://doi.org/10.1088/1748-9326/aa723b, 2017.

741 Zscheischler, J., Orth, R. and Seneviratne, S.I.: A submonthly database for detecting changes
742   in vegetation-atmosphere coupling, Geograph. Res. Let., 42(22), 9816-9824,
743   doi:10.1002/2015GL066563, 2015.

744 **Tables**

745

746 **Table 1.** Main European drought events between 2001 and 2018 corresponding to the large

747 patterns in negative yield anomalies (< -1) observed in the maps reported in Fig. 2.

748 References to the scientific literature of each event are also report, with a brief description of

749 the document impacts for the agriculture sector.

Year of drought event	Area affected	Impacts for the agriculture sector	Reference
2003	Central Europe	Fall in EU cereal production of more than 23 million tonnes as compared to 2002. Also fodder deficit ranging between 30% and 60%.	Rebetez et al. (2006); De Bono et al., 2004.
2005	Iberia Peninsula	Cereal production reduced to 60% of average and severe shortage of wheat (more than 50% in Portugal).	García-Herrera et al. (2007); Gouveia et al. (2009).
2006	North-Eastern Europe	Crop yield losses and forest fires in Lithuania. About 20% yield reduction for all cereals in Poland.	Valiukas (2015); Somorowska (2016); Sassenrath et al. (2012).
2007	Eastern Europe	The drought destroyed 60% of the cereal crops in Romania, and lowest recorded	Bogdan et al. (2008); Sima et al. (2015); Demuth (2009).

		yields in some counties. Estimated economic costs of at least 1.5 billion Euros.	
2012	Eastern Europe	About 5.9 million hectares of crops impacted all over Romania.	Sima et al. (2015)
2017	Southern Europe	Reduction in agricultural production, especially for cereals (among other crops) in Spain and Italy, with estimated losses of 2 billion euros in Italy.	García-Herrera et al. (2019)
2018	Central-Northern Europe	Yield reductions from 9% to 50% for the main crops.	Buras et al. (2020); Toreti et al. (2019)

750

751 **Figures**

752
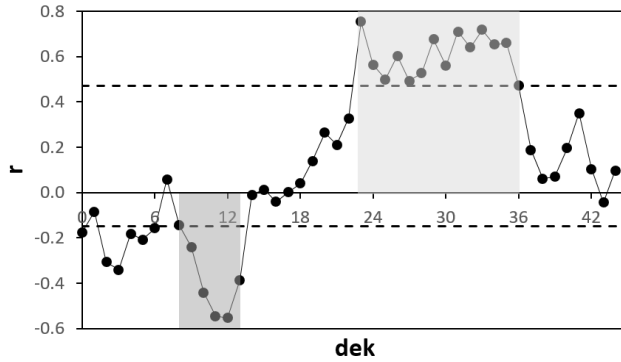
753

754 **Fig. 1.** Example of correlogram for one NUTS 2 region in Italy (ITI1, Tuscany). Each value
755 represents the Spearman correlation coefficient between the fAPAR anomaly time series of a
756 specific dekad and the yearly yield anomalies. The two horizontal dashed lines represent,
757 respectively, the threshold for positive statistical significant value at $p = 0.05$ and the
758 minimum negative threshold ($r = -0.15$, see the main text). Dekads are defined starting from
759 the first one of October of the previous year (e.g. dek $= 23$ refers to the last dekad of May of
760 the current year).
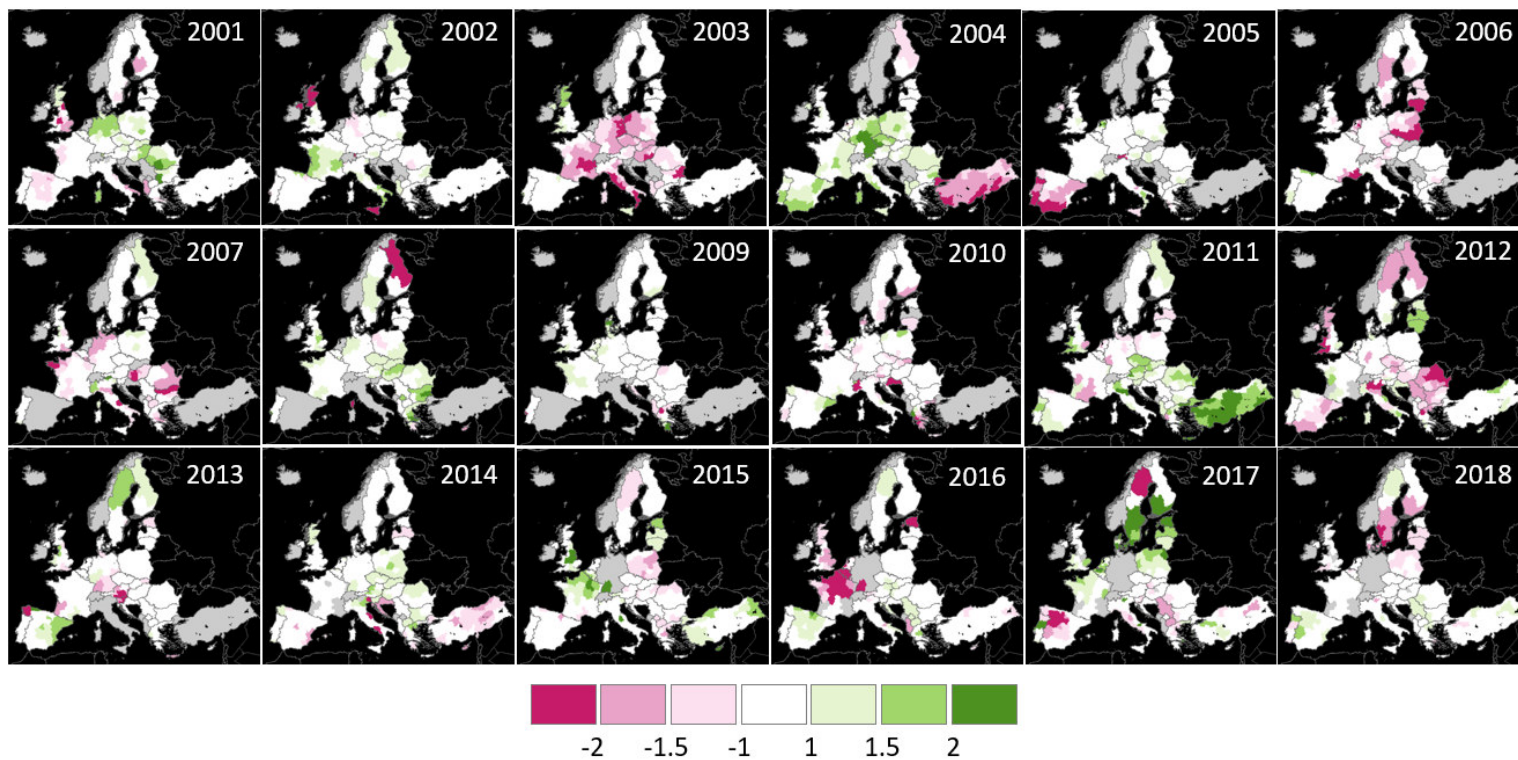
761
Fig. 2. Spatial distribution of annual standardized yield anomalies for the period 2001-2018. Anomalies are mapped at NUTS 2 level, with the
exception of the areas detailed in Section 2.1. Data in grey are missing.
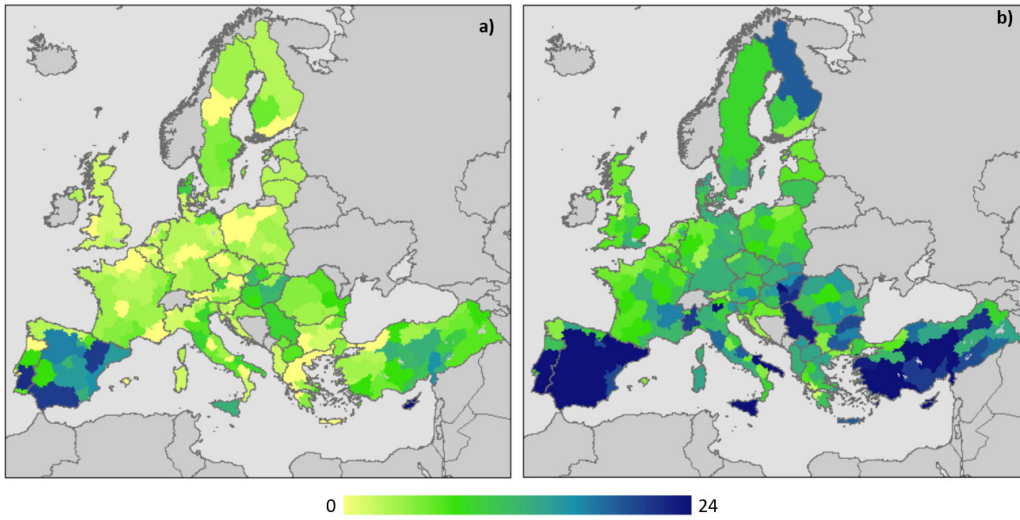
764

765 **Fig. 3.** Spatial distribution of the length (in dekads) of the longest period with $F_{p+} = 1$ (panel

766 a) and $F_+ = 1$ (panel b).

767
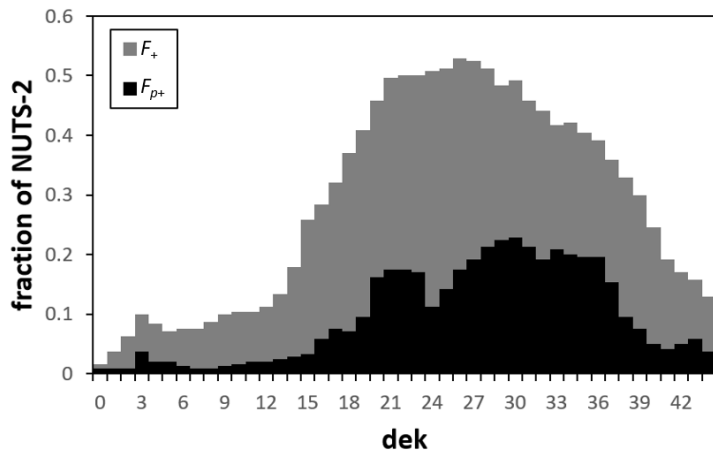
768 **Fig. 4.** Fraction of NUTS 2 regions for which each dekad is included in the longest

769 homogeneous period with $F_{p+} = 1$ (black) or $F_+ = 1$ (grey).

770

771 **Fig. 5.** Spatial distribution of the length (in dekads) of the longest period with $F_{p-} = 1$ (panel

772 a) and $F_{-} = 1$ (panel b).

773
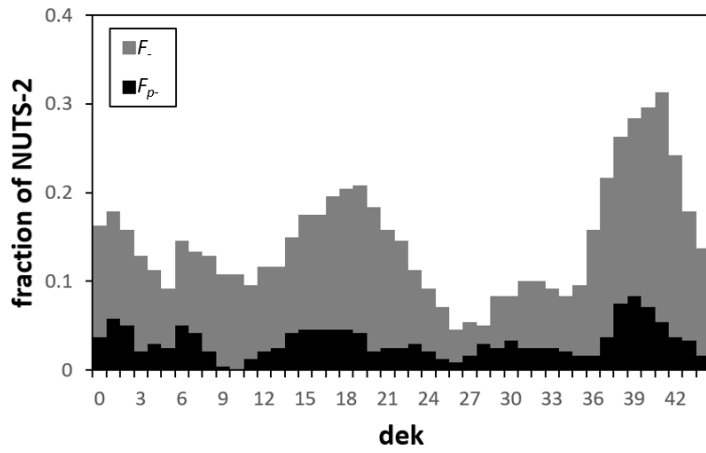
Fig. 6. Fraction of NUTS 2 regions for which each dekad is included in the longest

homogeneous period with $F_{p-} = 1$ (black) or $F_- = 1$ (grey).
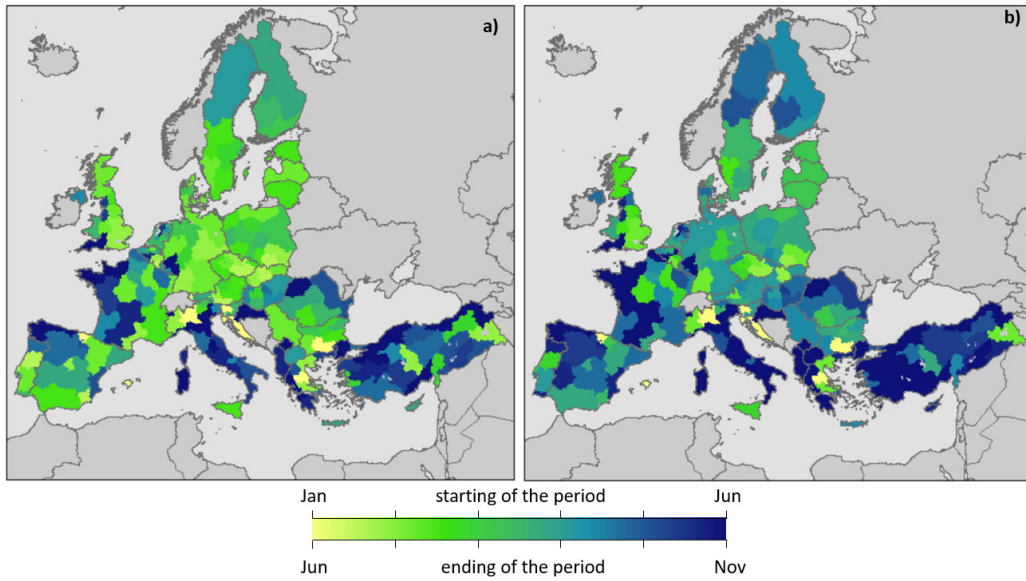
Fig. 7. Spatial distribution of (a) the starting dekad, and (b) the ending dekad, of the local optimal period based on the average correlation and bounded by a length from 6 to 8 months.
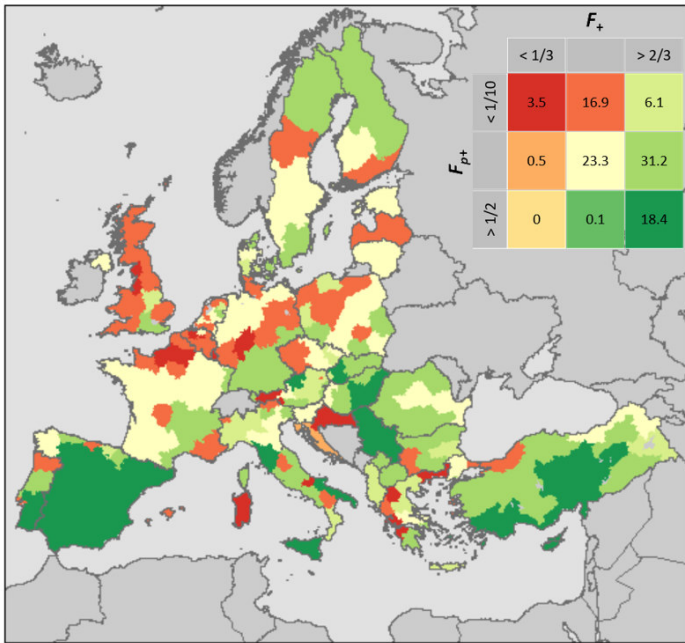
779

780 **Fig. 8.** Synthetic representation of the performance of dekadal fAPAR anomalies in
781 reproducing the yearly yield variations during the local optimal period. The inserted legend
782 shows the values of F_{p+} and F_+ for each category, with the numbers inside each square
783 representing the percentage (%) of the total NUTS 2 regions (out of 240) that falls under each
784 category.

785
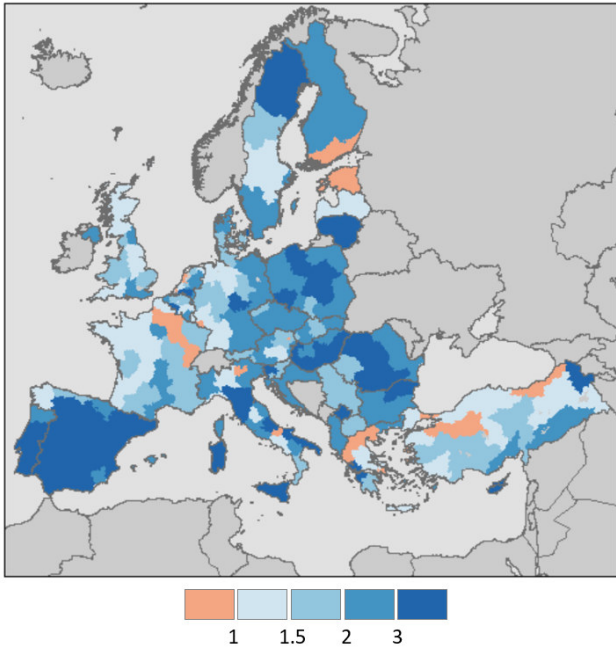
Fig. 9. Spatial distribution of the ratio between the number of fAPAR anomalies < -1 in the

optimal period (see section 3.3) during low yield years (yield anomalies < -1) and other years
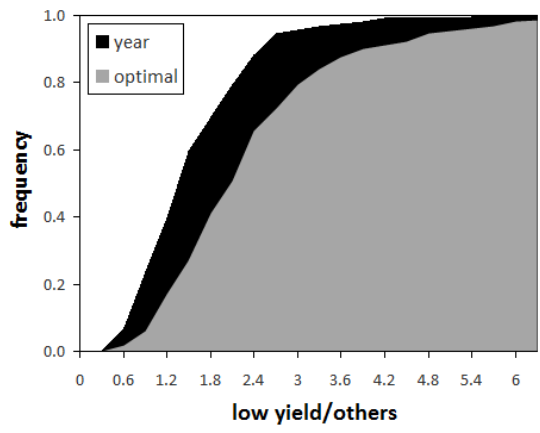
(yield anomalies ≥ -1).

789

790 **Fig. 10.** Cumulated frequency of: i) the ratio between the number of fAPAR anomalies < -1 in

791 the optimal period (see section 3.3) during low yield years (yield anomalies < -1) and other

792 years (yield anomalies ≥ -1) (optimal, grey area); and ii) the ratio between the number of

793 fAPAR anomalies < -1 in the full year (36 dekads) during low yield years and other years

794 (year, black area).